UC San Diego

UC San Diego Previously Published Works

Title

Transient temperature and water distributions in unconstrained compacted granular bentonite under elevated temperatures

Permalink

https://escholarship.org/uc/item/3kf093cd

Authors

Lu, Yu

McCartney, John S

Publication Date

2025-03-01

DOI

10.1016/j.gete.2024.100626

Copyright Information

This work is made available under the terms of a Creative Commons Attribution License, available at https://creativecommons.org/licenses/by/4.0/

Peer reviewed

eScholarship.org Powered by the California Digital Library
University of California

Revised manuscript (clean version) Click here to view linked References

Transient Temperature and Water Distributions in Unconstrained Compacted Granular Bentonite under Elevated Temperatures

Yu Lu, Ph.D. (corresponding author)

Postdoctoral Researcher, Dept. of Structural Engineering, Univ. of California San Diego, 9500 Gilman Dr., La Jolla, CA 92093-0085; yu-lu@ucsd.edu

John S. McCartney, Ph.D., P.E., F.ASCE

Professor and Hal Sorenson Endowed Chair, Dept. of Structural Engineering, Univ. of California San Diego, 9500 Gilman Dr., La Jolla, CA 92093-0085; mccartney@ucsd.edu

Abstract: This paper focuses on understanding transient temperature and water redistributions in compacted bentonite under thermal gradients in high-level nuclear waste disposal repository, particularly during the initial drying of granular bentonite with localized water content and volume changes near the canister. One-dimensional heating tests were conducted to investigate the coupled thermal-hydraulic-mechanical (THM) response of compacted granular MX80 bentonite layers under unconstrained and globally constant water content conditions during basal heating, encompassing both prolonged heating processes followed by natural cooling. Measurements of the transient temperature and volumetric water content redistributions at different vertical distances from the basal heating plate under high-temperature gradients and the global volumetric strains reveal varying rates of heat transfer and water vapor diffusion processes and associated volume change. A hysteretic relationship between volumetric water content and soil temperature during heating and cooling was found to be linked to soil water retention mechanisms. Temperature and water content relationships with local axial strains were found to be useful in evaluating density gradient changes that may occur near the canister.

Keywords: MX80 bentonite; Buffer systems; Thermal gradient; Cyclic heating; Hysteresis

1. Introduction

Compacted bentonite, with low permeability, high exchange capacity, sufficient swelling capacity, and adequate mechanical properties, is recognized as a suitable buffer material in geological repositories for high-level radioactive waste disposal[1-5]. During operation, the bentonite buffer may be exposed to prolonged elevated temperatures resulting from nuclide decay within the canister, leading to the formation and redistribution of thermal and hydraulic gradients[6-9]. Temperature variations impact the hydraulic characteristics of the buffer system, including water retention, vapor diffusion, and permeability[10-11], while water content changes influence its thermal properties, like thermal conductivity and volumetric heat capacity[5,12,13]. Meanwhile, both temperature and water content fluctuations affect its mechanical behaviors, such as swelling pressure, compressibility, and strength[14-18], and other buffer performances, like gas and reactive transport[19,20], possible buffer and rock fracture[20,21], etc. Thus, understanding the temperature and water distribution in compacted bentonite under elevated temperatures is crucial, as it significantly impacts barrier system integrity and buffer performance. This insight is key for optimizing repository design, space utilization, and cost efficiency, as well as for determining the necessary interim storage periods. This paper focuses specifically on the thermo-hydro-mechanical (THM) behavior of an as-compacted granular bentonite element adjacent to the heater immediately after closure, prior to hydration from the host rock.

Numerous element-scale and full-scale experimental tests, covering a range of topics, including thermal conductivity[22,23], swelling[24,25], and mechanical behaviors[26,27], along with investigations into coupled THM behavior[28-31], have been conducted to explore the buffer performance of compacted bentonite. Results inform long-term buffer material simulations by guiding parameter selection, highlighting the need for understanding temperature effects on the coupled THM properties governing these processes. Although these studies have evaluated the

basic buffer performance of and reposority responses, the combined effects of heating, local water redistribution due to thermally induced water vapor diffusion, and volume changes in bentonite immediately after placement, before hydration, have not been thoroughly investigated. Moreover, prior experimental studies traditionally focused on ambient temperature or limited ranges, typically up to 80-90 °C. In contrast, current repository conditions are now considering waste canister temperatures that may reach as high as 200 °C[32-35]. Understanding high-temperature gradients is crucial, but the soil properties cannot be readily extrapolated from low-temperature data. For instance, thermal expansion, water redistribution, swelling potential, and chemical reactivity can exhibit significant non-linear differences and non-monotonic changes with temperature[36,37].

Full-scale tests are valuable for capturing real-world repository construction effects and boundary conditions. The recently initiated full-scale in-situ HotBENT[33] experiment (Fig. 1) is a good example, using heaters set to 175 and 200 °C and featuring various types of sensors. However, full-scale tests inevitably involve high installation and operating costs. Meanwhile, mock-up or tank-scale tests, which are more cost-effective and easier to control, provide a practical alternative for studying repository behavior in a laboratory setting. For instance, Lu and McCartney[35] conducted tank-scale heating tests to investigate the coupled thermohydraulic behavior of compacted MX80 bentonite under a central heater temperature of 200 °C maintained by a cylindrical heating rod having a diameter of 12.5 mm. Temperature evolution and distribution at different positions within the central cross-section of the soil layers were captured by various kinds of sensors, but a notable radial-direction temperature drop, reaching approximately 75 °C at a distance of around 50 mm from the heater surface, was observed. A significant temperature reduction during heating tests on MX80 pellets at 140 °C was also observed by Gens et al.[38], whereas the FEBEX project reported a more distributed temperature decay away from the heater[26,29]. This discrepancy between laboratory and field tests provided

the motivation for better understanding the temperature and water distribution near a heater under high-temperature gradients.

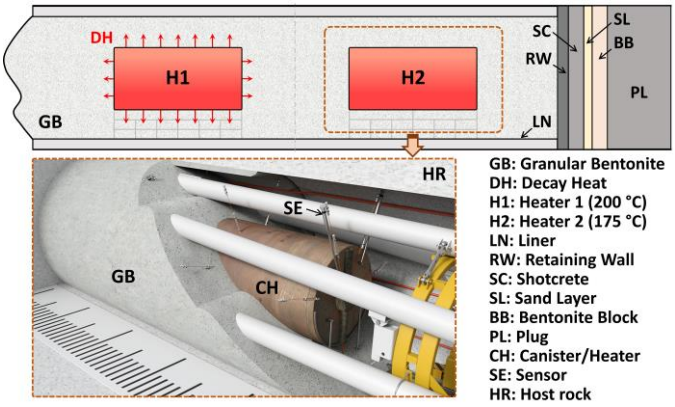

Fig. 1. Schematic diagram of HotBENT experiment in Grimsel Test Site (after Kober et al.[33]).

In this work, one-dimensional heating tests were conducted to investigate the coupled THM response of an MX80 bentonite layer under constant water content conditions (no drainage) and vertically unconstrained conditions, while maintaining a constant cross-sectional area. Tests involve basal heating with a constant thermal gradient followed by natural cooling and measurements include the transient temperature and volumetric water content redistribution at different vertical distances from the flat basal heating plate under high-temperature gradients as well as global volumetric strains. While the tests performed in this study do not fully replicate repository stress state and hydraulic boundary conditions, they represent a complex boundary value problem that can be used to validate numerical models and provide insight into coupled THM processes in an element of granular bentonite adjacent to the canister during initial drying leading to localized water content and density redistribution.

2. Material

The soil material used in this work is MX80 bentonite, sourced from Wyoming, a globally favored buffer for waste disposal projects[39-44]. The MX80 bentonite is comprised of primarily montmorillonite (85%), followed by quartz (6%), cristoballite (5%), clinoptiloite (2%), and biotite (2%), with a specific gravity of 2.76[45]. The Atterberg limits of this naturally occurring

bentonite are a liquid limit of 382, a plastic limit of 55, and a plasticity index of 327[37]. While Atterberg limits for bentonite can vary, the liquid and plastic limits here closely align with values reported by Tripathy et al.[46]. The grain size distribution curves of the bentonite in granular form using sieve testing and hydrated form using hydrometer testing are shown in Fig. 2. The granular form exhibits a relatively coarse grain size distribution, suggesting a distinction between macropores among granules and micropores within the granules. This disparity could potentially impact the thermo-hydraulic characteristics of the material. The scanning electron microscopy (SEM) of the MX80 bentonite with a dry density of 1.6 Mg/m^3 is shown in Fig. 3. SEM images reveal that aggregates are present in the compacted granular bentonite, with visible inter-aggregate pores.

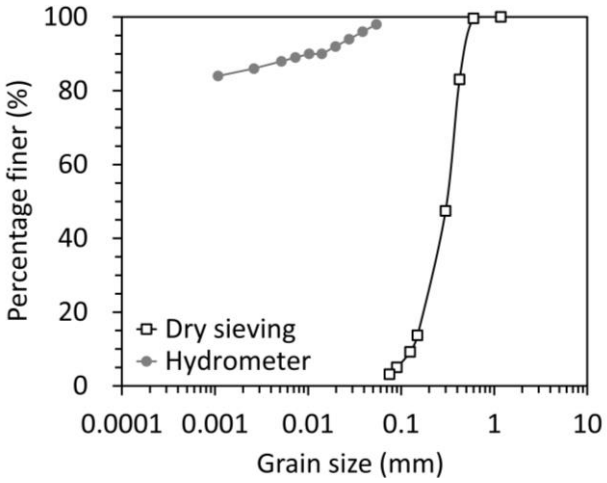

Fig. 2. Grain size distribution curves of MX80 bentonite.

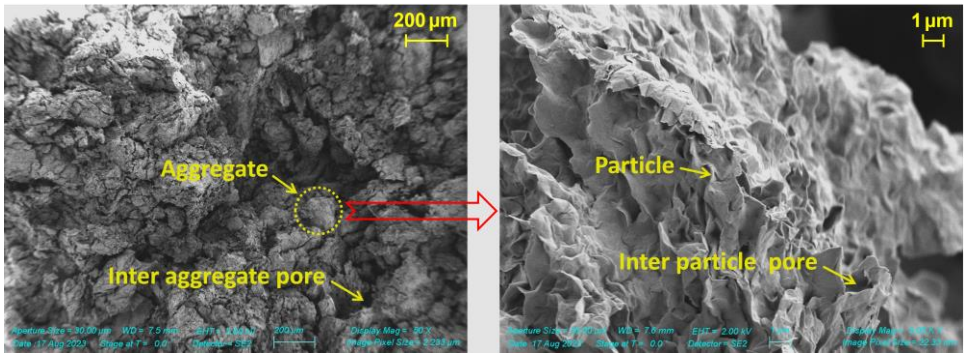

Fig. 3. SEM images of MX80 bentonite.

3. Experimental investigation

One-dimensional heating tests were performed on the granular MX80 bentonite layers in unconstrained conditions during basal heating, with globally constant water content but with local water redistribution. The experimental tests focus on assessing the coupled heat transfer and water flow processes related to the initial drying response of as-compacted granular bentonite immediately after placement, before groundwater infiltration occurs (which may take years to reach the bentonite near the canister). Basal heating was applied using a heating plate (Fig. 4) and embedded dielectric sensors were used to measure the transient redistribution in temperature and volumetric water content at different vertical distances from the heating plate under high-temperature gradients as along with the global volumetric strain by a dial indicator.

Two tests with various thermal paths were conducted to investigate transient temperature and water redistribution within the compacted bentonite: I) constant thermal gradient; and II) thermal cycling after an initial heating period. Test I is designed to investigate the long-term (10000 hours) evolution of thermal and hydraulic parameters, while Test II focuses on studying the soil's thermal response during cyclic heating and cooling. In the first stage of Test II, 4000 hours of constant temperature heating are performed, serving as confirmatory testing for Test I. Following this, the THM process during natural cooling was evaluated under laboratory conditions. In both Tests I and II, dielectric sensors (5TM sensors from Decagon Devices of Pullman, WA, with an accuracy of ±1 °C in temperature and ±0.02 in volumetric water content) were placed into an unsaturated compacted granular MX80 layer within a PVC modified Proctor mold (inner diameter of 152 mm, height of 178 mm, and coefficient of thermal expansion of 3.38×10^{-5}/°C), as shown in Fig. 4.

Bentonite with its natural water content, e.g., 10~15%, is commonly used when constructing buffer systems. In this study, the initial gravimetric water content of the granular bentonite is 13.5%, maintained in a relative humidity controlled container in the laboratory,

which corresponds to a total suction of approximately 71 MPa. The target height of the bentonite layer was 178 mm, achieved through compaction in four lifts for greater homogenization, which also accommodates the location of the dielectric sensors (Fig. 4). The compaction conditions for the soil layer and sensor locations are presented in Table 1. A wide range of dry densities for bentonite buffer materials has been explored in the literature, with the granular bentonite typically placed loose, e.g., 1.26~1.46 Mg/m^3 for the DECOVALEX project (Gens et al.[47]). A relatively low dry density of 1.25 Mg/m^3 was chosen for this work to minimize the influence of compaction stress history/OCR and to prevent sensor deformation or damage.

Low-density polyethylene sheeting was stretched across the top and bottom of the soil layers to minimize any global loss of water from the compacted bentonite layer during heating. A temperature-controlled heating plate was used as the basal heat source, and a dial indicator was mounted on the top of the soil layer to measure volume changes. Fiberglass insulation, with a thermal conductivity of 0.46 W/(m·K) and a heat capacity of 700 J/(kg·K), was wrapped around the cell to minimize lateral heat loss from the side boundary. Note that radial thermal deformation is expected to occur on the mold, which may have a minor influence on soil volume measurements. However, this effect is not considered in this work due to its negligible impact compared to soil volume deformation in the axial direction where the confinement is minimal.

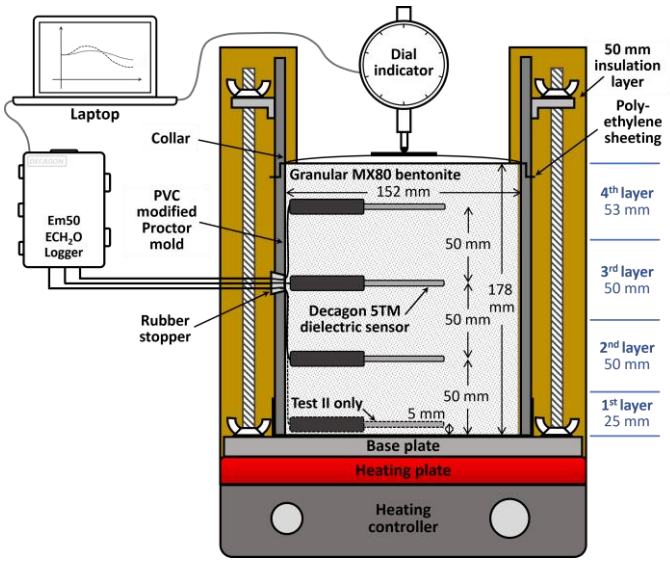

153

154 **Fig. 4.** Schematic diagram of the testing system.

155 **Table 1.** Initial conditions of the soil layer after preparation

Parameter	Test I					Test II				
	L1	L2	L3	L4	Total	L1	L2	L3	L4	Total
h (mm)	25.0	50.0	50.0	53.0	178.0	25.0	50.0	50.0	53.0	178.0
ω (%)	13.50	13.50	13.51	13.50	13.50	13.50	13.49	13.50	13.50	13.50
ρ (Mg/m^3)	1.68	1.68	1.67	1.68	1.68	1.66	1.67	1.66	1.66	1.66
ρ_d (Mg/m^3)	1.25	1.25	1.24	1.25	1.25	1.23	1.24	1.23	1.23	1.23
θ (m^3/m^3)	0.17	0.17	0.17	0.17	0.17	0.17	0.17	0.17	0.17	0.17
e (m^3/m^3)	1.21	1.21	1.22	1.21	1.21	1.24	1.23	1.24	1.24	1.24
n (m^3/m^3)	0.55	0.55	0.55	0.55	0.55	0.55	0.55	0.55	0.55	0.55

156 Note: h is layer thickness; ω is gravimetric water content; ρ is density; ρ_d is dry density; θ is
157 volumetric water content; e is void ratio; n is porosity.
158

159 ## 4. Results and analysis

160 ### 4.1. Constant thermal gradient results

161 The long-term soil temperature evolutions at three locations (50, 100 and 150 mm from
162 the base plate) during the first constant thermal gradient heating with a basal temperature of
163 125 °C (Test I) are shown in Fig. 5(a) on a natural timescale, revealing that soil temperatures
164 initially increase rapidly and then gradually stabilize. Meanwhile, the developments of soil
165 temperatures at four locations (5, 50, 100 and 150 mm from the base plate) during the constant

thermal gradient heating stage (heating only stage, first 4000 hours) in Test II are plotted in Fig. 5(b), and the data is presented on a semi-logarithmic coordinate system to highlight the time dependence during the initial phase of heating, offering a clearer view of the early-stage temperature changes. Results indicate a sharp, non-linear increase in temperature during the first ten hours, followed by a stabilization phase. Note that the data for the sensor located 5 mm from the base plate was lost after reaching approximately 110 °C, but the clear sharp, non-linear temperature increase, which was the earliest among the four locations, was recorded and plotted prior to that. Meanwhile, a minor temperature drop was observed at 100 mm and 150 mm, likely due to an approximate 2 °C decrease in ambient laboratory temperatures.

Similarly, the time-series evolution of the volumetric water content for Test I and Test II are plotted in Figs. 6(a) and 6(b), respectively. It is evident that the volumetric water content starts to increase when heating begins, but after a period of heating, it starts to decrease gradually. The initial increase in water content occurs because the water near the basal heating plate diffused upward during heating, resulting in a temporary wetting front that passes by the sensors. Over time, the wetting front is followed by gradual drying of the bentonite corresponding to a decrease in water content. The curves at different locations follow similar trends, but the degree of change and the turning point is influenced by the distance from the heating source. Specifically, for the location closest to the heating plate (5 mm from the base plate), the curve is the first to exhibit non-monotonic changes, with an inflection point occurring quickly, after approximately 2 hours of heating (Fig. 6b). For the location 50 mm from the base plate, a significant increasing-decreasing trend an inflection point occurring around 10 hours of heating was observed, and it has the greatest amplitude of variation. In contrast, at the location farthest from the heating plate (150 mm from the base plate), the curve is the last to exhibit changes, with a slow increase occurring after several hours of heating, followed by a slight decrease over hundreds or even thousands of hours of heating.

Compared with the temperature time series from these sensors in Fig. 5, the water content continues to decrease (Fig. 6) even after the temperature at this location has stabilized, indicating that the heat transfer and water flow processes occurred at different rates. Meanwhile, for the long-term heating test (Figs. 5a and 6a), it is interesting to note that after an initial several hundred hours of heating, the volumetric water contents at locations of 50 mm and 150 mm from the base plate show minimal changes over the long term. However, at the 100 mm location, there is a notable decrease in water content after approximately 5000 hours of heating (Fig. 6a). The possible reason is that the bound water gradually is desorbed under the long-term high temperature application[8].

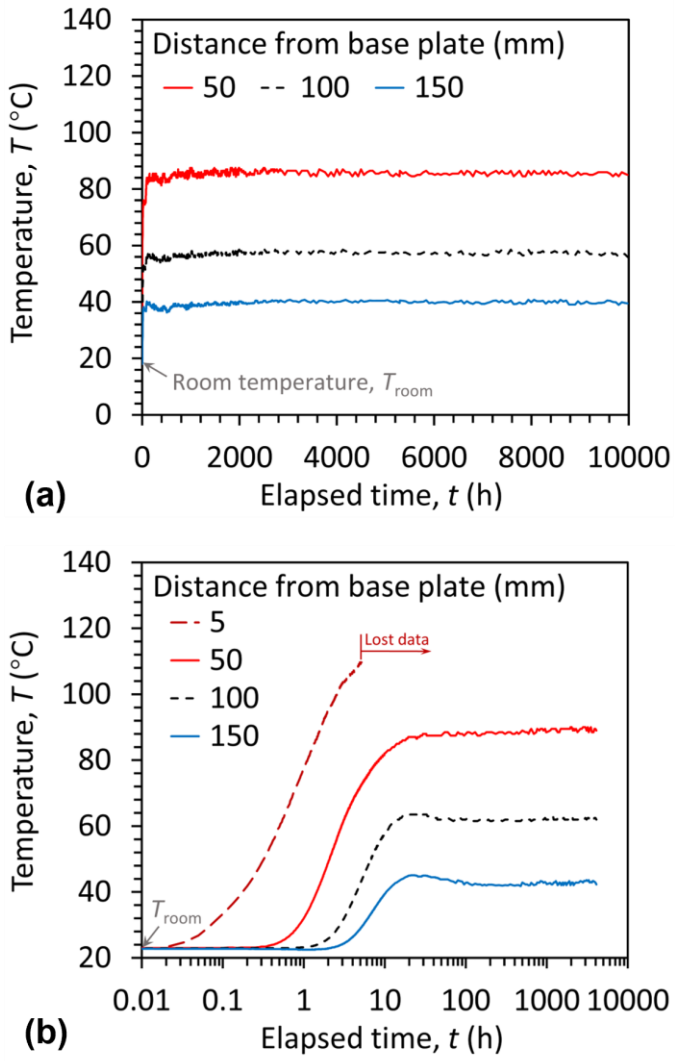

Fig. 5. Evolution of soil temperature: (1) Test I; (b) Test II

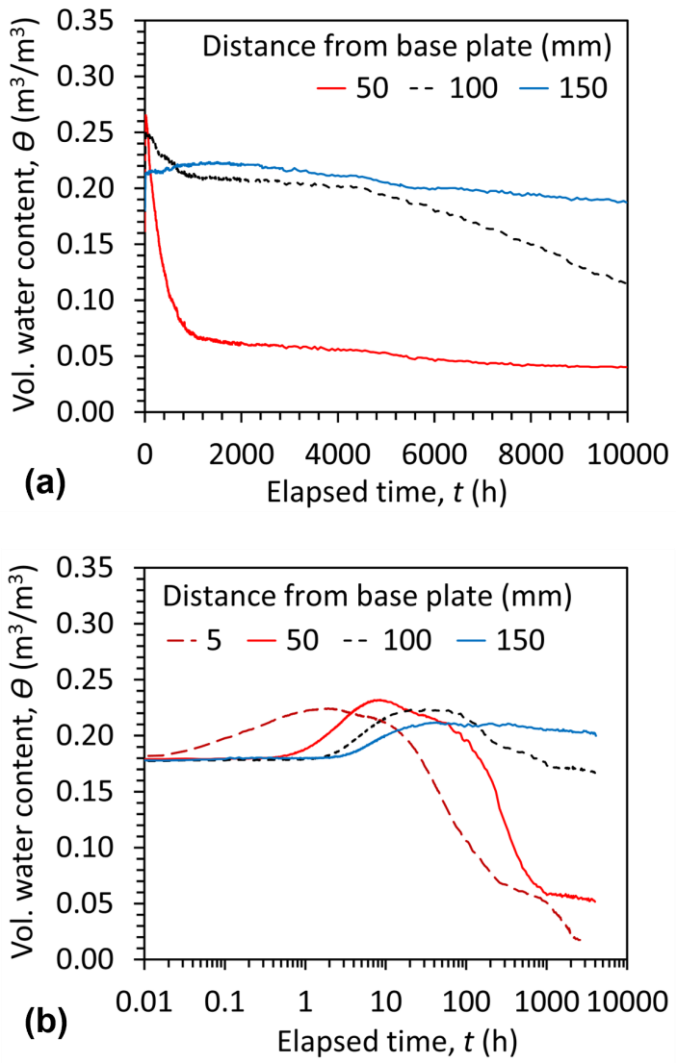

Fig. 6. Evolution of volumetric water content: (a) Test I; (b) Test II

The profiled distribution of temperature and volumetric water content of MX80 bentonite in long-term constant temperature heating are summarized in Fig. 7, along with the back-calculated volumetric water content derived from the gravimetric water content. For the gravimetric water content, five measurements were taken at different radial locations for each layer height, and the averaged values were used for calculations. Results demonstrated a nonlinear distribution of temperature and volumetric water content in MX80 bentonite under long-term constant temperature heating. The water content is much lower, though not zero, near the heating plate, while significantly higher water content is observed in areas farther from the heating plate. The volumetric water content profiles are not only helpful in understanding

the spatial distribution characteristics of temperature and hydraulic parameters governing heat transfer and thermally induced water flow but also provides a basis for subsequent volume change analysis. Meanwhile, the soil does not dry out fully after even after being exposed to temperatures above 100 °C for a significant time period.

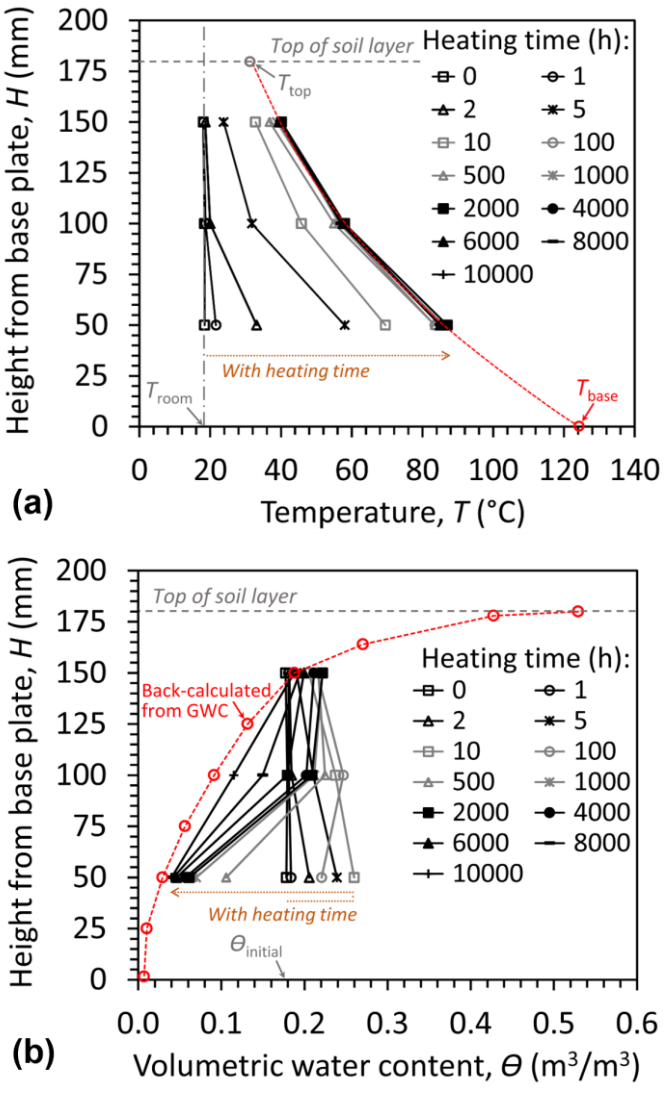

Fig. 7. Distribution of temperature and volumetric water content of MX80 bentonite in long-term constant temperature heating: (a) Temperature; (b) Volumetric water content from sensors and back-calculated from gravimetric sampling at the end of testing.

4.2. Heating-cooling response

After the initial 4000-hour heating period in Test II, the evolutions of soil temperatures and volumetric water content at various distances (50, 100, and 150 mm) from the base plate during

224 the natural cooling phase are shown in Figs. 8a and 8b, respectively. Note that the cooling phase
225 was initiated immediately thereafter the heating phase whose results are presented in Figs. 5b
226 and 6b. An interesting observation from the time series during natural cooling is that the
227 temperatures returned to their initial conditions but the volumetric water contents did not return
228 to the initial value of 13.5%, indicating that the upward thermally induced water vapor diffusion
229 process was not recoverable. A similar observation was made in the numerical simulations of
230 Baser et al.[48].

231 The relationship between volumetric water content and soil temperature upon heating and
232 cooling is plotted in Fig. 9. An increase in volumetric water content with increasing soil
233 temperature is observed at 100 mm and 150 mm from the base plate, mainly due to the
234 movement of the wetting front due to water vapor diffusion. In contrast, there is little change
235 at 50 mm from the base plate, as this area has experienced prolonged high thermal effects,
236 leaving little free water in the soil.

237 Moreover, a hysteresis on the evolution of water content between the heating and cooling
238 paths can be found in Fig. 9, with the effect being most noticeable at the closest location (50
239 mm) to the base plate where the soil holds higher suction and temperature. This behavior is
240 linked to the hysteresis of the soil water retention curve (SWRC) under wetting and drying
241 paths, which can be explained by changes in the solid-liquid-air contact angle mechanism[49,50].
242 Furthermore, for bentonite that consists of predominantly montmorillonite, the hydration at the
243 high suction range is mainly by interlayer exchangeable cation hydration mechanism, and
244 significant hysteresis between the drying and wetting SWRCs could be witnessed[51]. Higher
245 temperatures contribute to the desorption of water from the soil particle surfaces and
246 intercrystalline cations, and reduce the amount of water trapped in the pore space during
247 desorption[11,52].

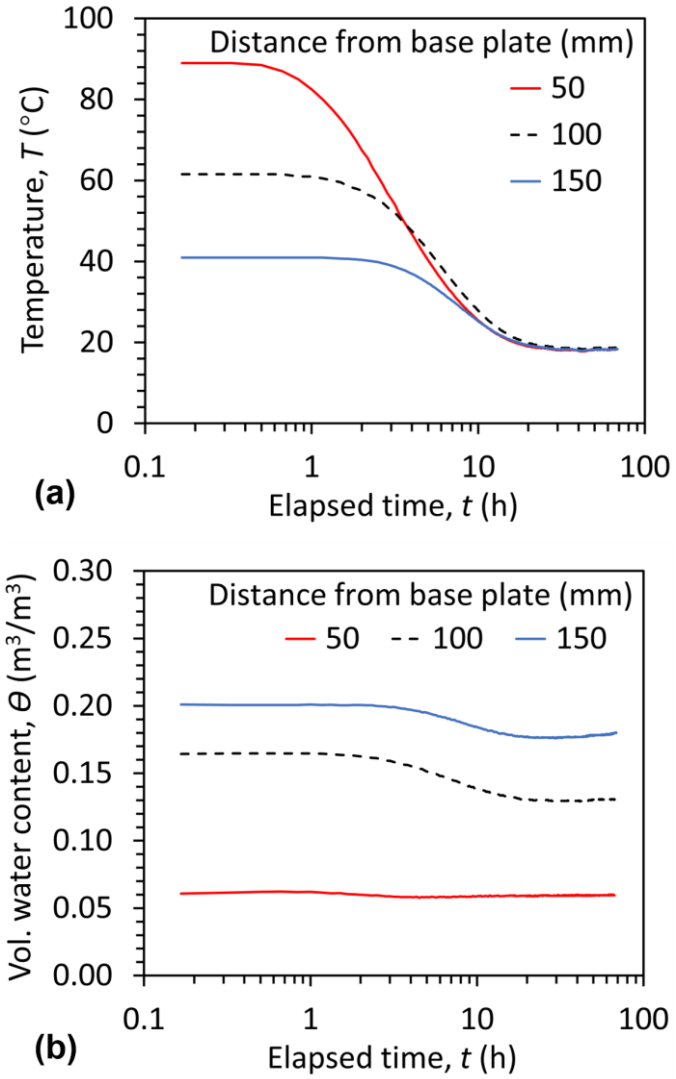

248

249 **Fig. 8.** Evolution of soil temperature and volumetric water content during cooling at different

250 locations from the base plate: (a) temperature; (b) volumetric water content.

251

252

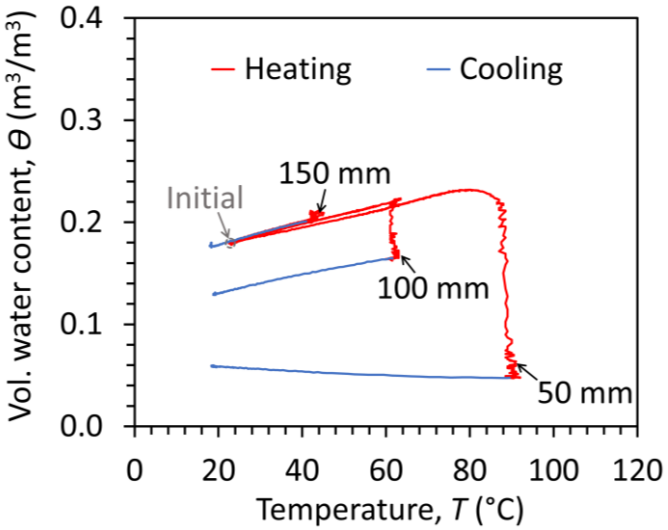

Fig. 9. Hysteretic relationships between volumetric water content and soil temperature at different locations from the base plate from Test II

4.3. Volumetric behavior

The evolution of volumetric strain in compacted bentonite under constant temperature heating in Tests I and II are shown in Fig. 10. Meanwhile, the volumetric strain data from Lu and McCartney[34] for the granular MX80 bentonite with a similar dry density (1.3 Mg/m^3) under central heating at 200 °C is also included. Besides, since the figure is intended to compare volumetric strain during heating, the cooling phase in Test II is not included. The curves under constant heating stages of Tests I and II nearly overlap, demonstrating the similarity of the two test results. Results reveal an initial increase in volumetric strain (swelling), followed by a decrease (contraction) as heating progressed. The thermal expansion is expected for an over-consolidated soil[53,54]. Nonetheless, the volumetric strains observed for the soil layer were higher than those observed in Lu and McCartney[3534], but close to those observed by Tang and Cui[36].

In fact, the volume change behavior of bentonite under a thermal gradient can be induced by several factors, including water variation, heating duration, transformation of mineral composition, desorption of adsorbed water, micro-morphological changes, boundary conditions, etc. In the scope of this paper, reversible phenomena at the aggregate level can be

related to the expansion of the mineralogical components and the remaining adsorbed water and to physicochemical changes induced on diffuse double layers[55]. The arrangement of the macrostructure of the clay skeleton is irreversibly affected during the first heating by these changes in aggregate volume. However, irreversible effects on clay skeletons are not only due to aggregate thermal expansion. In addition, increasing temperatures appear to generate structural disturbance of the interlayer water lattice in montmorillonite, inducing aggregate contraction on heating due to a denser grouping of stacks of flakes and favoring the transition from adsorbed water to free water[56-58].

The MX80 bentonite contains montmorillonite as the dominant mineral and water in various forms with differing densities[8], including strongly bound water which is primarily in the form of crystalline water associated with hydrophilic compounds on the mineral surface (1.3–2.4 Mg/m^3), weakly bound water that typically found in the diffusion layer of clay colloids (1.2–1.8 Mg/m^3), and free water (≈1.0 Mg/m^3). Previous research indicated that free water can be desorbed from MX80 bentonite at temperatures ranging from 30 to 80 °C, while weakly bound water can be desorbed at 80 to 145 °C, and strongly bound water typically requires a higher temperature range for desorption.

In the heating tests under high-temperature gradients, the water transfer from the intra-aggregate space to the inter-aggregate pores can enhance the expansion at first due to the change of water form and density. However, extended heating and high-temperature gradients cause water in the soil to gradually transfer, leading to soil shrinkage. During heating at high temperatures, it is hypothesized that free water, weakly bound water, and possibly some strongly bound water are desorbed and lost through evaporation, resulting in a reduction of crystal layer spacing. This leads to contraction and deformation between the lamellar minerals, ultimately inducing internal microstructural variations in the bentonite.

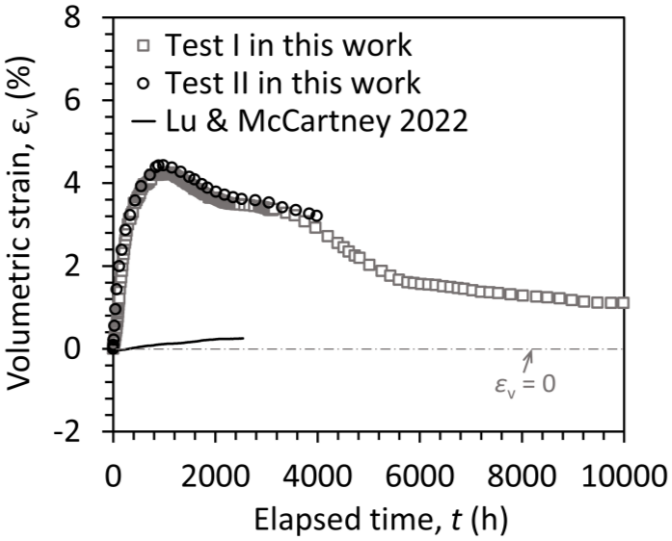

296

297 **Fig. 10.** Volumetric strain evolution of MX80 bentonite layer during heating.

298 **5. Discussion**

299 **5.1. Heating element size effect**

300 The stabilized temperature distribution in MX80 bentonite with distance from the base
301 plate after 4000 hours of basal heating tests (with heating plate) is shown in Fig. 11, along with
302 central heating tests (with heating rod) on MX80 bentonite and Bonny silt. Results in the figure
303 reveal a smoother temperature gradient in the work (Tests I and II), compared to the sharp drop-
304 off observed in the literature using a 12.5 mm diameter cartridge heating element. For instance,
305 in the central heating test performed by Lu and McCartney[34], even though the temperature at
306 the center of the heater was 200 °C, due to the low thermal conductivity of the bentonite along
307 with three-dimensional heat transfer effects (i.e., upward and downward heat transfer in
308 addition to radial heat transfer as expected in the repository), the soil temperature at the location
309 of the sensor (20 mm away) only approached 80 °C (Fig. 12). A similarly sharp temperature
310 drop was witnessed on the compacted Bonny silt by Behbehani and McCartney[59], as shown in
311 Fig. 11, possibly attributable to the utilization of a smaller-sized heater and the continuous
312 expansion of the cross-sectional area of the soil.

313 Although a similar phenomenon was also reported by Gens et al.[38] for heating tests on

MX80 pellets during heating to 140 °C, measurements from the FEBEX project indicate a more distributed temperature decay away from the heater[29]. The surface area of the heater in contact with the surrounding bentonite significantly impacts temperature distribution and coupled water flow. This finding can help guide the geometric design of small-scale laboratory experiments studying THM processes under controlled conditions. In other words, to accurately reflect the actual operating environment in a buffer system within a repository, it is necessary to consider the size effect in experiments.

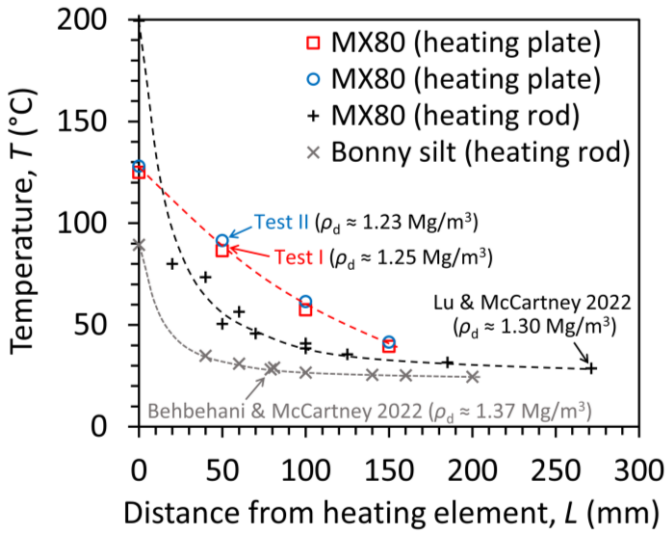

Fig. 11. Temperature distribution and comparison with literature data.

5.2. Volume change evaluation

The volume change of expansive soil upon heating involves two mechanisms: thermal skeleton expansion and suction-induced swelling/contraction. Correspondingly, an equation describing the change in void ratio is developed in this work, as follows:

$$e(T,\psi) = \alpha_T \cdot (T - T_0) + \beta_\psi \cdot \ln\left(\frac{\psi}{\psi_0}\right) + e_0 \quad (1)$$

where e is the void ratio at temperature T and suction ψ, e_0 is the initial void ratio (about 1.12), T_0 and ψ_0 are the initial temperature (around 22 °C) and suction (approximately 97 MPa); α_T is the thermal expansion coefficient, varies with soils, and a value of 3.4×10^{-5} °C^{-1} is stated for clay by McTigue[60] and Delage[61], and also adapted in this work; β_ψ is a soil-related swelling

index, and a linear relationship between the void ratio and suction is adapted for simply. A similar linear relationship between the void ratio and suction in a semi-log space for bentonite or bentonite/sand mixtures under free swelling conditions has been observed by previous researchers[16,62-64]. Note that Eq. 1 is an empirical formula applicable to the high suction range associated with density redistribution during initial drying of as-compacted granular bentonite near a heat source, and additional test data is needed to establish a more general relationship addressing a broader suction range and other stress states.

Based on the measured soil temperature and volumetric water content (Figs. 5 and 6), the suctions at corresponding locations can be calculated using the SWRC[65,66]. Recently, Lu and McCartney[11] proposed a non-isothermal SWRC that considers temperature effects on adsorption and capillarity water retention mechanisms, as follows:

$$\theta(\psi,T)=\theta_{\mathrm{a}}(\psi,T)+\theta_{\mathrm{c}}(\psi,T) \tag{2}$$

$$\theta_{\mathrm{a}}=\theta_{\mathrm{a,max}}(T)\left\{1-\left[\exp\left(\frac{\psi-\psi_{\mathrm{max}}(T)}{\psi}\right)\right]^{M}\right\} \tag{3}$$

$$\begin{aligned}\theta_{\mathrm{c}}=\frac{\theta_{\mathrm{s}}-\theta_{\mathrm{a}}}{2}&\left\{1-\mathrm{erf}\left[\sqrt{2}\frac{\psi}{\psi_{\mathrm{c}}(T)}\left(\frac{\chi(T)+T}{\chi_{\mathrm{r}}+T_{\mathrm{r}}}\right)-\sqrt{2}\right]\right\}\\&\cdot\left\{1+\left[\alpha\psi\left(\frac{\chi(T)+T}{\chi_{\mathrm{r}}+T_{\mathrm{r}}}\right)\right]^{N}\right\}^{1/N-1}\end{aligned} \tag{4}$$

where $\theta(\psi)$ is the (volumetric) water content (m^3/m^3) corresponds to the suction ψ, $\theta_a(\psi)$ and $\theta_c(\psi)$ represent the water content (m^3/m^3) corresponds to the adsorption and capillary mechanism respectively, ψ_{max} is the maximum matric suction (kPa) which corresponding to the endpoint of the SWRC when the water content is zero, ψ_c is the mean cavitation suction (kPa) that is associated with the physical-phase transition point between the adsorption and capillarity mechanisms, θ_s is saturated water content (m^3/m^3) equal to porosity of the soil, $\theta_{a,max}$ is the adsorption capacity (m^3/m^3) which corresponds to the maximum water content contributed by the adsorption mechanism, M is the adsorption strength (dimensionless) that controls the

changing rate of adsorption near the maximum matric suction and is only controlled by mineral type and quantity and bears little relation to pore size distribution, N is capillary pore-size distribution parameter (dimensionless) that controls the curve slope in the capillary regime, T is temperature in Kelvin, T_r is the reference temperature (K), χ is the temperature correction factor (K), χ_r is the temperature correction factor at reference temperature (K), α is the reciprocal of the air entry suction (1/kPa) which is associated with the inflection point of the SWRC at high water content range, and erf() is the error function. More details can be found in Lu and McCartney[11]. The SWRC model in Eqs. 2-4 has been validated on different types of highly plastic clayey soils, including MX80 bentonite, and was thus adopted in this work. The estimated suctions based on the model for different locations are plotted in Fig. 12. The hysteretic evolution between the wetting and drying paths of the SWRC is shown in Fig. 12b. Once again, the wetting path is due to the movement of the wetting front at the beginning of heating, while the drying path corresponds to the subsequent heating stage.

The simulated local strain for Test II according to Eq. 1 (with β_ψ value of -0.105) is shown in Fig. 13. This approach allows for evaluating density gradient changes, which are difficult to measure accurately, based on the local strain (volume change) behavior observed in the test. The basic SWRC parameters at ambient room temperature are listed in Table 2, while the detailed derivation processes and parameter determination methods can be found in Lu and McCartney[11]. Note that the effect of local density changes on the SWRC is not considered, as it has been found to have a minor effect at low degrees of saturation[67]. The total strain (general volume change) can be obtained by integrating local strain, as shown by the black dashed line in Fig. 13, demonstrates a similar swelling-contraction trend to the measured axial strain in Fig. 10. Although the temperature and volumetric water content profiles (e.g., Fig. 7) provide estimates at different locations, parameter acquisition at various locations is still encouraged.

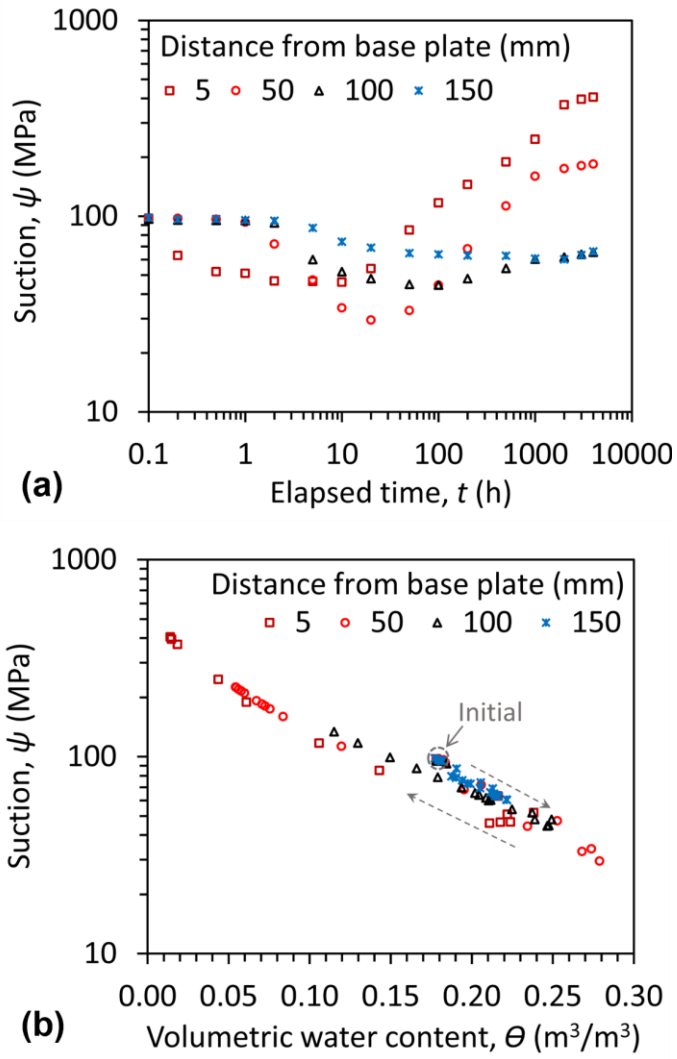

374

375 **Fig. 12.** Estimated suctions based on non-isothermal SWRC of Lu and McCartney[11]: (a) time

376 series evolution; (b) estimated suction vs. measured volumetric water content.

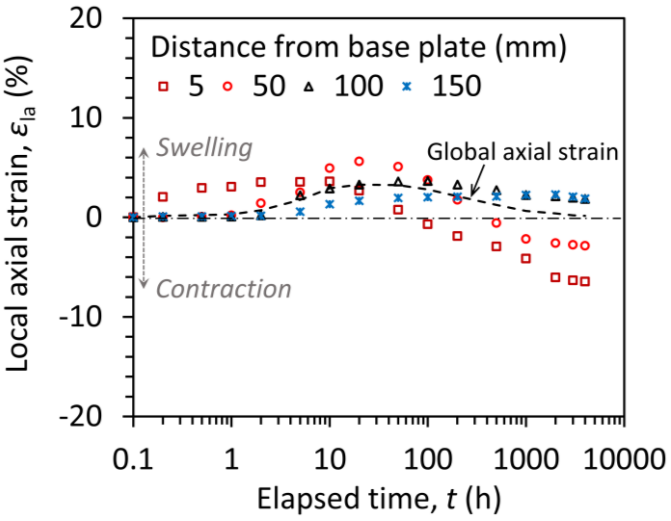

377

378 **Fig. 13.** Simulated local strains at different locations upon heating.

Table 2. SWRC model parameters for MX80 bentonite at room temperature

Parameter	Adsorption			Capillarity			
	ψ_{max} (MPa)	$\theta_{a,max}$ (m^3/m^3)	M (-)	ψ_c (MPa)	α (1/kPa)	χ (K)	N (-)
Value	903	0.306	0.105	10.2	0.0012	341.2	1.27

Furthermore, the evolution of local strain with temperature at different locations reveals a non-monotonic change, with initial expansion (swelling) followed by contraction (Fig. 14). Similar expansion-contraction behavior has been observed in other over-consolidated soils, including Boom clay[53] and Bonny silt[68], etc. It is noted that the local strain is higher than that in these two types of soils, possibly due to the dominance of montmorillonite in MX80, which has significant water retention ability and induces substantial volume changes in response to suction changes[17,46,69], especially under unconfined conditions[16,37].

Although initial void ratio and compaction conditions have been found not to strongly affect the thermal volume change results[68,70], the thermal volume evolution of compacted, unsaturated soils is complex and can be influenced by various parameters and testing paths. Thermoelastic expansion can be interpreted in terms of thermal expansion of the solid phase, while for plastic contraction, different mechanisms have been used to explain the results, ranging from thermally induced pore water pressure dissipation to thermal collapse and thermally accelerated creep (Coccia and McCartney[70]). Among these mechanisms, the role of water absorbed along the clay particles is crucial for bentonite. There could be a process that separates the adsorbed water from the clay particles (plastic), along which they are bonded, by squeezing out during heating. This can be verified by the continuous decrease in water content when the soil temperature is stable (see Figs. 5 and 6). While some results suggest that an elasto-plastic model with suction hardening and thermal softening may be applicable, some others are inconsistent.

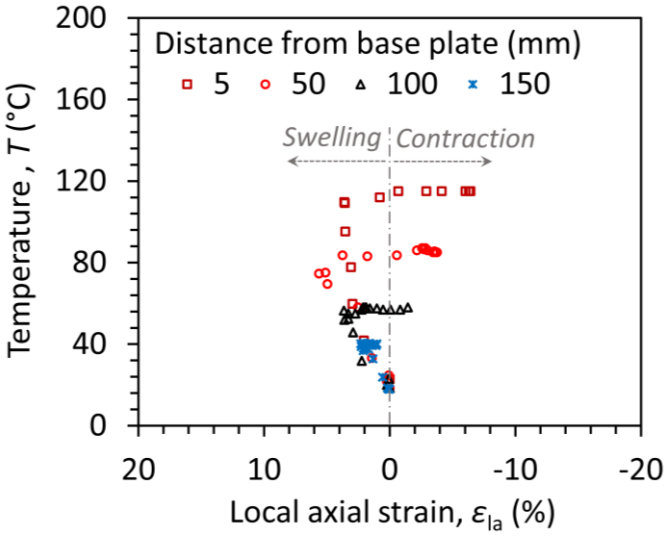

401

402 **Fig. 14.** Evolution of local strain with temperature during heating.

403 **6. Conclusion**

404 One-dimensional heating tests on unsaturated compacted granular bentonite under
405 unconstrained and constant water content conditions were conducted to investigate transient
406 temperature and water distributions during prolonged periods of constant thermal gradient
407 basal heating and heating-cooling processes. Measurements include the transient temperature
408 and volumetric water content redistribution at different vertical distances from the flat plate
409 heater under high-temperature gradients as well as global volumetric strains.

410 Results for a granular bentonite having an initial gravimetric water content of 13.5% and a
411 low dry density of approximately 1.25 Mg/m^3 showed that heat transfer and water flow
412 processes occurred at different rates. The soil temperature increases notably during the initial
413 stages of heating before gradually stabilizing. A wetting front was observed to initially move
414 away from the bottom soil layer near the basal heating plate due to thermally induced water
415 vapor diffusion, followed by a long-term drying process. Hysteresis in water content during
416 thermal cycles was observed and was found to be linked to the soil water retention mechanism.
417 The testing approach proposed in this study can also be used to evaluate the initial heating
418 response of bentonites under other different initial compaction conditions, including those
419 prepared using pelletized bentonite to reach higher dry densities.

Another finding of this study is that the heater's surface area in contact with the surrounding bentonite significantly affects temperature distribution and coupled water flow. Density gradient changes, which are difficult to measure accurately, can be evaluated based on the local volume change behavior observed in the test. These findings may provide insights for the geometric design of small-scale laboratory mock-up experiments used to study THM processes in controlled laboratory conditions.

Declaration of Competing Interest

The authors declare that they have no known competing financial interests or personal relationships that could have appeared to influence the work reported in this paper.

Data Availability

All data used in this study is reported within the paper.

Acknowledgements

The authors appreciate support from U.S. Department of Energy's Nuclear Energy University Program award DE-NE008951. The views herein are those of the authors alone.

References

1. Pusch R. Use of bentonite for isolation of radioactive waste products. *Clay Miner*. 1992;27(3):353–361.
2. Tripathy S, Thomas HR, Bag R. Geoenvironmental application of bentonites in underground disposal of nuclear waste: characterization and laboratory tests. *J Hazard Toxic Radioact Waste*. 2017;21(1):D4015002.
3. Darde B, Dangla P, Roux JN, Pereira JM, Talandier J, Vu MN, Tang AM. Modelling the behaviour of bentonite pellet-powder mixtures upon hydration from dry granular state to saturated homogeneous state. *Eng Geol.* 2020;278:105847.
4. Bosch JA, Qiao Y, Ferrari A, Laloui L. Thermo-hydro-mechanical analysis of the complete lifetime of the bentonite barrier in the FEBEX in-situ test. *Geomech Energy Environ*.

2023;34:100472.

5. Lu Y, McCartney JS. Thermal conductivity function for fine-grained unsaturated soils linked with water retention by capillarity and adsorption. *J Geotech Geoenviron Eng.* 2024;150(1):06023009.
6. Villar MV, Lloret A. Influence of temperature on the hydro-mechanical behaviour of a compacted bentonite. *Appl Clay Sci*. 2004;26(1–4):337–350.
7. Villar MV, Gómez-Espina R, Lloret A. Experimental investigation into temperature effect on hydro-mechanical behaviours of bentonite. *J Rock Mech Geotech Eng*. 2010;2(1):71–78.
8. Zeng Z, Shao J, Sun DA, Lyu H, Xu Y, Yang C. Effect of thermal ageing on physical properties of MX80 bentonite under high-temperature conditions. *Eng Geol*. 2022;308:106822.
9. Zheng L, Fernández AM. Prediction of long-term geochemical change in bentonite based on the interpretative THMC model of the FEBEX in situ Test. *Minerals*. 2023;13(12):1522.
10. Cho WJ, Lee JO, Chun KS. The temperature effects on hydraulic conductivity of compacted bentonite. *Appl Clay Sci*. 1999;14(1–3):47–58.
11. Lu Y, McCartney, JS. Temperature effects on adsorption and capillarity water retention mechanisms in constrained unsaturated soils. *Acta Geotech.* 2024; https://doi.org/10.1007/s11440-024-02341-9.
12. Ye W, Lu Y, Huang X, Chen B, Chen Y, Cui Y. Anisotropic thermal conductivity of unsaturated compacted GMZ bentonite-sand mixture. 2017. In *PanAm Unsaturated Soils 2017* (pp. 413–424).
13. Chen T, Fei W, Narsilio G. Effective thermal conductivity of granular soils: a review of influencing factors and prediction models towards an investigation framework through multiscale characters. *Can Geotech J.* 2024. https://doi.org/10.1139/cgj-2023-0465.

14. Vinšová H, Jedináková-Křížová V, Kolaříková I, Adamcová J, Přikryl R, Zeman J. The influence of temperature and hydration on the sorption properties of bentonite. *J Environ Radioact.* 2008;99(2):415–425.
15. Yavari N, Tang AM, Pereira JM, Hassen G. Effect of temperature on the shear strength of soils and the soil–structure interface. *Can Geotech J.* 2016;53(7):1186–1194.
16. Zhu Y, Ye W, Wang Q, Lu Y, Chen Y. Anisotropic volume change behaviour of uniaxial compacted GMZ bentonite under free swelling condition. *Eng Geol*. 2020;278:105821.
17. Lu Y, Ye WM, Wang Q, Zhu YH, Chen YG, Chen B. Anisotropic swelling behaviour of unsaturated compacted GMZ bentonite hydrated under vertical stresses. *Bull Eng Geol Environ*. 2021;80(7):5515–5526.
18. Li A, Feng WQ, Chen ZJ, Mailk N, Yin JH, Zhou C. Investigation and analysis of the macro-and micro-responses of bentonite-sand mixtures to temperature. *Geomech Energy Environ*. 2024:100565.
19. Sedighi M, Thomas HR, Vardon PJ. Reactive transport of chemicals in compacted bentonite under nonisothermal water infiltration. *J Geotech Geoenviron Eng.* 2018;144(10):04018075.
20. Liaudat J, Dieudonné AC, Vardon PJ. Modelling gas fracturing in saturated clay samples using triple-node zero-thickness interface elements. *Comput Geotech.* 2023;154:105128.
21. Thomas HR, Vardon PJ, Cleall PJ. Three-dimensional behaviour of a prototype radioactive waste repository in fractured granitic rock. *Can Geotech J.* 2014;51(3):246–259.
22. Lu Y, Ye WM, Wang Q, Zhu YH, Chen YG, Chen B. Investigation on anisotropic thermal conductivity of compacted GMZ bentonite. *Bull Eng Geol Environ*. 2020;79:1153–1162.
23. Xu Y, Zhou X, Sun DA, Zeng Z. Thermal properties of GMZ bentonite pellet mixtures subjected to different temperatures for high-level radioactive waste repository. *Acta Geotech*. 2022;17:981–992.

24. Brachman RWI, Rowe RK, Baral A, Hosney MS, Su G, Nguyen TS, Brown J, Lange K. Bentonite swelling characteristics with a hypersaline multi-component pore fluid. *Can Geotech J*. 2021;58(3):367–376.
25. Lu Y, Ye WM, Wang Q, Chen YG. Insights into anisotropic swelling pressure of compacted GMZ bentonite. *Acta Geotech*. 2023;18:5721–5734.
26. Villar MV. *MX-80 Bentonite. Thermal-Hydro-Mechanical characterisation performed at CIEMAT in the context of the prototype project. CIEMAT-1053*. Madrid, Spain: Center for Energy, Environmental and Technological Research. 2005.
27. Sun DA, Zhang Q, Peng F. Effect of aging on shear strength of compacted GMZ bentonite. *Eng Geol*. 2022;302:106632.
28. Åkesson M, Jacinto AC, Gatabin C, Sanchez M, Ledesma A. Bentonite THM behaviour at high temperatures: experimental and numerical analysis. *Géotechnique*. 2009;59(4):307–318.
29. Villar MV, Martín PL, Bárcena I, García-Siñeriz JL, Gómez-Espina R, Lloret A. Long-term experimental evidences of saturation of compacted bentonite under repository conditions. *Eng Geol*. 2012;149:57–69.
30. Manca D, Ferrari A, Laloui L. Fabric evolution and the related swelling behaviour of a sand/bentonite mixture upon hydro-chemo-mechanical loadings. *Géotechnique.* 2016;66(1):41–57.
31. García-Siñeriz JL, Mazón MR, Kober F, Sakaki T. Performance of THM monitoring instrumentation in FEBEX bentonite barrier after 18 years of operation under repository-like conditions. *Geomech Energy Environ*. 2019;17:75–89.
32. Zheng L, Rutqvist J, Birkholzer JT, Liu HH. On the impact of temperatures up to 200 °C in clay repositories with bentonite engineer barrier systems: A study with coupled thermal, hydrological, chemical, and mechanical modeling. *Eng Geol*. 2015;197:278–295.

33. Kober F, Schneeberger R, Vomvoris S, Finsterle S, Lanyon B. The HotBENT Experiment: objectives, design, emplacement and early transient evolution. *Geoenergy*. 2023;1(1):geoenergy2023-021.
34. Lu Y, McCartney JS. Physical modeling of coupled thermohydraulic behavior of compacted MX80 bentonite during heating. *Geotech Test J*. 2022;45(6):20220054.
35. Lu Y, McCartney, JS. Insights into the thermo-hydraulic properties of compacted MX80 bentonite during hydration under elevated temperature. *Can Geotech J*. 2024;61:344–360.
36. Tang AM, Cui YJ. Modelling the thermomechanical volume change behaviour of compacted expansive clays. *Géotechnique*. 2009;59(3):185–195.
37. Lu Y, McCartney, JS. Free swelling behavior of MX80 bentonite under elevated temperatures up to 200 °C. *Geomech Energy Environ*. 2024;37:100531.
38. Gens A, de Vasconcelos RB, Olivella S. Towards higher temperatures in nuclear waste repositories. In *E3S Web Conf* (Vol. 205, No. 01001, pp. 1–8). EDP Sciences. 2020.
39. Pusch R, Bluemling P, Johnson L. Performance of strongly compressed MX-80 pellets under repository-like conditions. *Appl Clay Sci*. 2003;23(1–4):239–244.
40. Ferrari A, Seiphoori A, Rüedi J, Laloui L. Shot-clay MX-80 bentonite: An assessment of the hydro-mechanical behaviour. *Eng Geol.* 2014;173:10–18.
41. Dieudonné AC. *Hydromechanical behaviour of compacted bentonite: from micro-scale analysis to macro-scale modelling*. University of Liege. 2016.
42. Gatabin C, Talandier J, Collin F, Charlier R, Dieudonné AC. Competing effects of volume change and water uptake on the water retention behaviour of a compacted MX-80 bentonite/sand mixture. *Appl Clay Sci.* 2016;121:57–62.
43. Dieudonne AC, Della Vecchia G, Charlier R. Water retention model for compacted bentonites. *Can Geotech J.* 2017;54(7):915–925.
44. Eizaguirre P, Tang AM, Maillet B, Sidi-Boulenouar R, Talandier J, Pereira JM, Vu MN,

Chabot B, Dangla P, Bornert M, Aimedieu, P. Exploring two regimes of water mobility in unsaturated expansive clay using NMR relaxometry. *Appl Clay Sci.* 2024;251:107324.

45. Müller-Vonmoos M, Kahr G. *Mineralogische untersuchungen von wyoming bentonit MX-80 und Montigel*. 1983. Nagra Technischer Bericht 83-12.

46. Tripathy S, Bag R, Thomas HR. Effects of post-compaction residual lateral stress and electrolyte concentration on swelling pressures of a compacted bentonite. *Geotech Geol Eng*. 2014;32(4):749–763.

47. Gens A, Alcoverro J, Blaheta R, Hasal M, Michalec Z, Takayama Y, Lee C, Lee J, Kim GY, Kuo CW, Kuo WJ, Lin CY. HM and THM interactions in bentonite engineered barriers for nuclear waste disposal. *Int J Rock Mech Min Sci*. 2021;137:104572.

48. Başer T, Dong Y, Moradi AM, Lu N, Smits K, Ge S, Tartakovsky D, McCartney JS. Role of nonequilibrium water vapor diffusion in thermal energy storage systems in the vadose zone. *J Geotech Geoenviron Eng*. 2018;144(7), 04018038.

49. Johnson Jr RE, Dettre RH. Contact angle hysteresis. III. Study of an idealized heterogeneous surface. *J Phys Chem.* 1964;68(7):1744–1750.

50. Likos WJ, Lu N. Hysteresis of capillary stress in unsaturated granular soil. *J Eng Mech.* 2004;130(6):646–655.

51. Lu N, Khorshidi M. Mechanisms for soil-water retention and hysteresis at high suction range. *J Geotech Geoenviron Eng.* 2015;141(8):04015032.

52. Revil A, Lu N. Unified water isotherms for clayey porous materials. *Water Resour Res.* 2013;49(9):5685–5699.

53. Sultan N, Delage P, Cui YJ. Temperature effects on the volume change behaviour of Boom clay. *Eng Geol.* 2002;64(2–3):135–145.

54. Cekerevac C, Laloui L. Experimental study of thermal effects on the mechanical behaviour of a clay. *Int J Numer Anal Meth Geomech.* 2004;28(3):209–228.

55. Morin R, Silva AJ. The effects of high pressure and high temperature on some physical properties of ocean sediments. *J Geophys Res.* 1984;89(B1):511–526.
56. Ma C, Hueckel T. Stress and pore pressure in saturated clay subjected to heat from radioactive waste: a numerical simulation. *Can Geotech J.* 1992;29:1087–1094.
57. Ma C, Hueckel T. Thermomechanical effects on absorbed water in clays around a heat source. *Int J Numer Anal Methods Geomech.* 1993;17:175–196.
58. Zhang F, Zhang ZZ, Low PF, Roth CB. The effect of temperature on the swelling of montmorillonite. *Clay Miner.* 1993;28:25–31.
59. Behbehani F, McCartney JS. Energy pile groups for thermal energy storage in unsaturated soils. *Appl Therm Eng.* 2022;215:119028.
60. McTigue DF. Thermoelastic response of fluid-saturated porous rock. *J Geophys Res.* 1986;91(B9):9533–9542.
61. Delage P. On the thermal impact on the excavation damaged zone around deep radioactive waste disposal. *J Rock Mech Geotech Eng.* 2013;5(3):179–190.
62. Delage P, Howat MD, Cui YJ. The relationship between suction and swelling properties in a heavily compacted unsaturated clay. *Eng Geol.* 1998;50:31–48.
63. Al-Mukhtar M, Qi Y, Alcover JF, Bergaya F. Oedometric and water-retention behavior of highly compacted unsaturated smectites. *Can Geotech J.* 1999:36:675–684.
64. Gatabin C, Talandier J, Collin F, Charlier R, Dieudonné AC. Competing effects of volume change and water uptake on the water retention behaviour of a compacted MX-80 bentonite/sand mixture. *Appl Clay Sci.* 2016;121–122:57–62.
65. Olson RE, Daniel DE. Measurement of the hydraulic conductivity of fine-grained soils. *ASTM STP. Permeability and Groundwater Contaminant Transport.* 1981;746:18–64.
66. Fredlund DG, Sheng DC, Zhao, JD. Estimation of soil suction from the soil-water characteristic curve. *Can Geotech J.* 2011;48(2):186–198.

595 67. Romero E, Gens A, Lloret A. Suction effects on a compacted clay under non-isothermal
596 conditions. Géotechnique, 2003;53(1):65–81.
597 68. Alsherif NA, McCartney JS. Nonisothermal behavior of compacted silt at low degrees of
598 saturation. *Géotechnique.* 2015;65(9):703–716.
599 69. Saiyouri N, Tessier D, Hicher PY. Experimental study of swelling in unsaturated compacted
600 clays. Clay Miner. 2004;39(4):469–479.
601 70. Coccia CJR, McCartney JS. Thermal volume change of poorly draining soils I: Critical
602 assessment of volume change mechanisms. *Comput Geotech.* 2016;80:26–40.
603